

Chapter 10

Muon Detectors

CDF has traditionally emphasized charged particle tracking and lepton identification. Triggering and reconstructing muons is at the core of several broad physics programs. Top quarks are identified in via muons from decays of their W and b daughters. W bosons are identified in part and their mass measured via their muon decay mode. Systematic effects in the W mass measurement are studied with the large sample of $J/\psi \rightarrow \mu^+ \mu^-$ decays, a sample that is also central to the CDF B physics program. The asymmetry in W decays constrains parton distribution functions, and many signatures of new physics involve one or more leptons.

In Run I and before, there was a logical distinction between central muons and forward muons. Central muons were identified by their penetrating ability, and detected by chambers located outside substantial material. The momentum of these muons was measured by measuring their bend in the solenoidal field using the central trackers. Forward muons were identified and their momentum measured simultaneously in toroidal magnets in the forward region.

With the improved tracking system of CDF II, especially the inner silicon, momentum resolution in the forward region for high p_T tracks is similar for the solenoid and the toroids. The distinction between “central” and “forward” muons is now purely historic; *all* muons will be identified by their passage through material and have their momentum measured using the solenoid.

The existing central muon systems have performed well in the present run. We are planning a program of incremental improvements rather than major replacements of the detectors. Our goals are to preserve and improve the existing detector performance under the new operating conditions in the Main Injector era.

The existing forward muon system (FMU) is built around two pairs of toroids, one pair at positive rapidity, the other at negative. There are electrode-

less drift chambers installed between the toroids and on the outer and inner faces of the toroids, and two planes of scintillation counters. Details of the design and construction of the FMU can be found in [1]. The FMU has fewer channels per unit rapidity, and therefore higher occupancy, than the central detectors. At luminosities of $1.0 \times 10^{32} \text{ cm}^{-2}/\text{s}$, the detectors could be made to function with substantial effort, but above that, and certainly by $2.0 \times 10^{32} \text{ cm}^{-2}/\text{s}$, muon reconstruction would have been severely degraded. Extrapolations from Run I data estimate reconstruction efficiencies of 70% and below at high luminosities.

For the $|\eta| > 1$ region in Run II, CDF has elected to cover a smaller and lower rapidity interval ($\eta = 1.0 - 1.5$) with sufficient granularity to survive high luminosity, by a) pushing the toroids as close to the central detector as possible, and b) building a cylindrical “barrel” of chambers (with chambers as staves of this barrel) similar to the existing central chambers around the outside radii of the toroids and c) installing scintillation counters for triggering and identifying which beam crossing generated the muon of interest. The design closely parallels that of the central detectors. The 1.0-1.5 region was chosen because:

- It covers more solid angle than the region covered by the original FMU, even in the pushed-up position. For high mass objects such as $t\bar{t}$ pairs and energetic lepton pairs used to constrain quark substructure, solid angle is the figure of merit, not rapidity.
- The W asymmetry is largest in this region.
- The region is contiguous with the existing central detectors.

Between $\eta = 1.5$ and $\eta = 2.0$ there is also muon identification, with granularity (and therefore occupancy) insufficient for triggering, but adequate for identifying high p_T tracks in this region as muons.

There will be four detectors for muon identification in Run II. We summarize design parameters of detectors in Table 10.1. In Sections 10.1, 10.2, and 10.3,

we describe them as they are now. In Sections 10.4 and 10.5, we identify the changes in the detector and read-out planned for Run II. Section 10.6 describes the changes and new detector construction in the $\eta > 1.0$ region. Finally, Section 10.7 contains a discussion of performance issues related to higher luminosities and different bunch structures.

10.1 Central Muon Detector

The CMU, the original set of muon chambers, consists of 144 modules with 16 rectangular cells per module, located behind $\sim 5.5\lambda$ of absorber (the Central Hadron Calorimeter). Each cell is $6.35 \times 2.68 \times 226$ cm in size and has a $50 \mu\text{m}$ stainless steel wire in the center. The 16 cells in a module are stacked four deep in the radial direction, with a small ϕ offset between the first and third and second and fourth layers. The first and third (and second and fourth) ϕ cells have their wires ganged together in the read-out, and each wire pair is instrumented with a TDC to measure the muon's location in ϕ , and an ADC on each end to measure the muon's location in z via charge division.

Table 10.1 lists some design parameters of the CMU.

Further information about the CMU detector can be found in Ref. [2].

10.2 Central Muon Upgrade

The Central Muon Upgrade (CMP) consists of a second set of muon chambers behind an additional 60 cm of steel in the region $55^\circ \leq \theta \leq 90^\circ$. The chambers are of fixed length in z and form a box around the central detector. The pseudo-rapidity coverage thus varies with azimuth as shown in Figure 10.1. The return yoke of the CDF solenoid provides the necessary steel above and below the central detector. Steel has been added on the two sides in the form of two non-magnetized retractable walls. Table 10.1 lists some design parameters of the CMP.

The central upgrade chambers are rectangular, single-wire drift tubes configured in four layers with alternate half-cell staggering. For easy field shaping, the drift cell design cross-section has a 3:1 aspect ratio ($2.5 \text{ cm} \times 15 \text{ cm}$). The chambers are run in proportional mode with a maximum drift time of approximately $1.4 \mu\text{s}$.

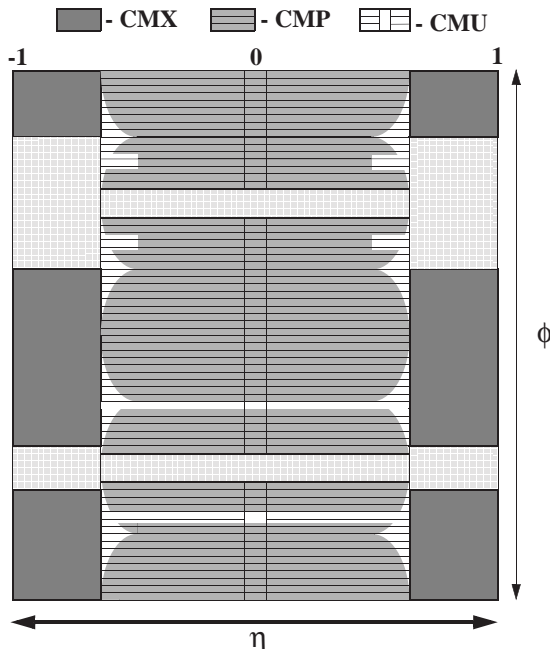


Figure 10.1: Location of the Run I muon upgrade components in azimuth ϕ and pseudorapidity η . The gray cross-hatched region indicates the currently uninstrumented regions of CMP and CMX.

The tubes are made of aluminum extrusions with 0.26 cm walls, having a single wire in the center and field shaping cathode strips on the top and bottom. They are typically 640 cm long, with some shorter sections on the bottom of the detector to avoid obstructions. The extrusions are glued into four-tube stacks with a half-cell staggering of the second and fourth layers relative to the first and third. Preamplifiers are mounted on one end of the stacks. Signals are read out by a single TDC per wire, and trigger hits are formed from coincidences of nearby wires that are used in association with trigger information from the CMU chambers.

A layer of scintillation counters (the CSP) is installed on outside surface ¹ of the wall drift chambers. The counters are rectangular in shape: $2.5 \text{ cm} \times 15 \text{ cm} \times 320 \text{ cm}$. Each counter covers two upgrade chambers in width and half the chamber length. The total number of scintillation counters is 216. The counters are read out by single phototubes which are located at the center of the array. The east and west

¹with respect to the interaction point

	CMU	CMP/CSP	CMX/CSX	IMU
Pseudo-rapidity coverage	$ \eta \leq \sim 0.6$	$ \eta \leq \sim 0.6$	$\sim 0.6 \leq \eta \leq \sim 1.0$	$\sim 1.0 \leq \eta \leq \sim 1.5$
Drift tube cross-section	2.68 x 6.35 cm	2.5 x 15 cm	2.5 x 15 cm	2.5 x 8.4 cm
Drift tube length	226 cm	640 cm	180 cm	363 cm
Max drift time	800 ns	1.4 μ s	1.4 μ s	800 ns
Total drift tubes (present)	2304	864	1536	none
Total drift tubes (Run II)	2304	1076	2208	1728
Scintillation counter thickness		2.5 cm	1.5 cm	2.5 cm
Scintillation counter width		30 cm	30-40 cm	17 cm
Scintillation counter length		320 cm	180 cm	180 cm
Total counters (present)		128	256	none
Total counters (Run II)		269	324	864
Pion interaction lengths	5.5	7.8	6.2	6.2-20
Minimum detectable muon p_T	1.4 GeV/c	2.2 GeV/c	1.4 GeV/c	1.4-2.0 GeV/c
Multiple scattering resolution	12 cm/p (GeV/p)	15 cm/p	13 cm/p	13-25 cm/p

Table 10.1: Design Parameters of the CDF II Muon Detectors. Pion interaction lengths and multiple scattering are computed at a reference angle of $\theta = 90^\circ$ in CMU and CMP/CSP, at an angle of $\theta = 55^\circ$ in CMX/CSX, and show the range of values for the IMU.

counters are offset in x to allow the inter-leaving of phototubes at the middle, minimizing the space occupied by the light-guide/PMT assembly.

Further information about the CMP detector can be found in Ref. [5].

10.3 Central Muon Extension

The central extension consists of conical sections of drift tubes (CMX) and scintillation counters (CSX) located at each end of the central detector and extending in polar angle from 42° to 55° . At 55° the CMX/CSX system slightly overlaps the coverage provided by the central muon system and extends its pseudorapidity coverage from 0.65 to 1.0. No additional steel was added for this detector; however, as seen in Figure 10.2, the large angle through the hadron calorimeter, magnet yoke, and steel of the detector end support structure yields considerably more absorber material on average than in the original central muon system. Table 10.1 lists some design parameters of the CMX and CSX detectors.

The azimuthal coverage of CMX/CSX has a 30° gap at the top of the detector for the Tevatron Main Ring and the solenoid refrigerator. There is also a 90° azimuthal gap at the bottom of the detector where the conical sections are interrupted by the floor of

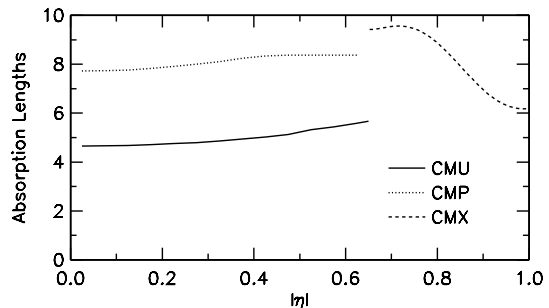


Figure 10.2: Number of absorption lengths as a function of pseudorapidity averaged over azimuthal acceptance of the CMU, CMP and CMX systems.

the collision hall. However, there is a narrow vertical gap between this section of floor and the bottom of the magnet yoke (see Fig. 10.6), and we plan to install a fan-shaped 90° CMX/CSX section in this gap completing the coverage at the bottom.

The CMX drift tubes are arrayed as a logical extension of the central system. There are four logical layers of twelve tubes for each 15° ϕ sector, and successive layers are half-cell offset to eliminate ambiguities. Each logical layer consists of two physical layers of drift tubes which partially overlap each other. The

overlap is greater at the inner edge of the detector as a result of forming a conical surface with rectangular cells. This overlap not only provides redundancy - the average muon intersects six cells - but the resulting stereo angle of 3.6 mrad between adjacent cells permits the measurement of the polar angle of the track.

The drift tubes for the CMX conical sections differ from those of the CMP only in length. They are 180 cm long. The total number of tubes installed in the conical sections of the central extension is 1536. The lower fan-shaped section will require 576 somewhat longer tubes when it is installed.

A layer of four CSX scintillation counters is installed on both the inside and the outside surfaces of each 15° CMX sector. The counters are trapezoidal in shape with the same length (180 cm) as the drift tubes and with a width of 30 cm at the smaller end and 40 cm at the larger end. The counters on the inside and outside layers are half-cell staggered with respect to each other thereby doubling the effective granularity of the system. The total number of scintillation counters in the conical sections is 256.

The counters are read out by single phototubes which are located on opposite ends for the inside and outside layers. The mean time of the signals from a particle traversing both layers is independent of the location of the track along the length of the counters, and the distribution of hit arrival time for real tracks is smeared only by the track path length difference due to the distribution of interaction z vertex. The mean time is calculated in the trigger, and the excellent timing resolution of the counters is used to reject large CMX backgrounds from out-of-time interactions in the beam pipe and the face of the forward calorimeter.

Further information about the CMX and CSX detectors can be found in Ref. [5].

10.4 Muon Detector Upgrades for Run II

For Run II, we plan to complete the coverage of the original muon upgrade projects as described in the 1990 CDF upgrade conceptual design[3] and to make other improvements as necessary to handle the shorter bunch-crossing time. We will add chambers to the Central Muon Upgrade and Central Muon Extension detectors to fill existing gaps. The final cov-

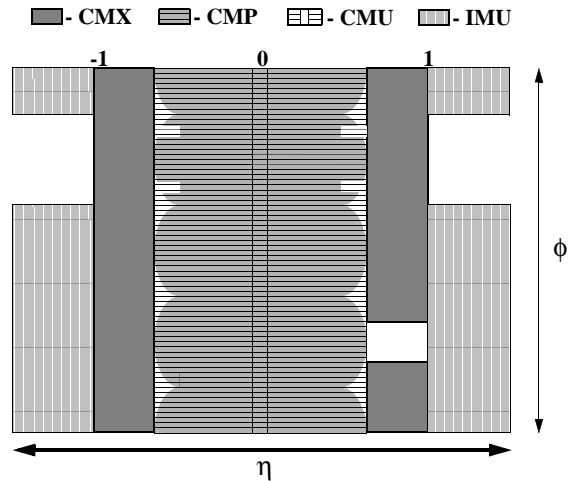


Figure 10.3: Location of the central muon upgrade components in azimuth ϕ and pseudorapidity η for Run II.

erage, shown in Fig. 10.4 (compare to Fig. 10.1) and listed in Table 10.4, will improve the acceptance of the CMP and CMX systems by 17% and 45% respectively. We will also add scintillation counters near the Central Muon Upgrade chambers to identify the beam crossing that produced the muon. These additions are described in Sections 10.4.1 and 10.4.2.

The gas gain of the Central Muon Detector will be reduced in Run II. This will require us to upgrade the the detector front-end electronics to handle the smaller signal. This is described in Sec. 10.5.1. The CMP/CSP and CMX/CSX front ends will not change, but we do plan to change the pre-amplifier motherboard system for the Central Muon Upgrade detector to improve operational efficiency and data quality (Sec. 10.5.2). This involves a change in the high voltage distribution and grounding scheme, not the pre-amplifier. Finally, a new TDC is necessary to accommodate the pipelined DAQ structure and to implement the trigger buffering scheme; this is described in Secs. 11.3-11.4.

10.4.1 Completion of the Central Muon Upgrade and Upgrade Scintillator

Completion of the Central Muon Upgrade (CMP) requires the following additional chambers and corresponding scintillator:

- Chambers to instrument the gap between the chambers on top of the north wall and those on

	CMU	CMP	CMX	CMUP	CM \bar{U} P	CMU \bar{P}	all
Run I	0.396	0.363	0.196	0.278	0.084	0.118	0.676
Run II	0.396	0.425	0.283	0.328	0.097	0.068	0.776
ratio	1.000	1.172	1.449	1.180	1.142	0.575	1.148

Table 10.2: Comparison of central muon detector acceptances in Runs I and II. Acceptance is computed for a 30 GeV/c muon with a uniform distribution in azimuth and pseudorapidity, $|\eta| < 1.2$, and no z vertex smearing. The changes due to a Gaussian z vertex distribution with $\sigma = 30$ cm are negligible (< 0.001). The CMUP region is the overlap between the CMU and CMP detectors; CM \bar{U} P is the region covered by CMP but not CMU, and CMU \bar{P} is the region covered by CMU but not CMP.

the north yoke

- Chambers to instrument the gap between the return yokes on the top
- Additional chambers to extend the coverage at the south end of the south yoke to cover the gap between the south yoke and the chambers on the top of the south wall
- Chambers to instrument the gap between the return yokes on the bottom

These additions will increase the CMP coverage by approximately 17%.

Additional steel is required in front of these chambers. The steel will be extended on the north side of the top north yoke and the south side of the top south yoke. Steel will be installed between the return yokes on the top and the bottom. (See Fig. 10.4). For this baseline design the number of additional chamber stacks required is 36 total.

There are mechanical complications with this design. On the north end, at the natural location for the chambers (i.e. the level of the yoke) there is an interference with the pivot for the large overhead cable tray. Furthermore, placing steel in the yoke gap precludes access to instrumentation for the central calorimeter in the two (notch) wedges. This problem already exists at the bottom, and is ameliorated by locating the readout electronics outside the notch, but occasional access to the PMTs on the wedges is still essential. On the bottom, necessary access is accomplished by pulling an arch, but this will not work at the top because the solenoid blocks lift access to the photomultiplier tubes.

We are now considering a different construction which would suspend the steel and chambers for this region from the ceiling. The primary issue with this

1 – Baseline design	
Distance from beam-line	186 in.
Width of steel absorber	75.3 in
Volume of steel absorber	263 ft ³
Equivalent length of MR shielding	241 in
Load replacement factor	N/A
2 – Installation above cable tray	
Distance from beam-line	228 in.
Width of steel absorber	92.4 in.
Volume of steel absorber	323 ft ³
Equivalent length of MR shielding	295 in.
Load replacement factor	1.2
3 – Installation at ceiling height	
Distance from beam-line	254 in.
Width of steel absorber	102.9 in.
Volume of steel absorber	360 ft ³
Equivalent length of MR shielding	329 in.
Load replacement factor	1.3

Table 10.3: Comparison of the absorber parameters for 3 different positions of the top CMP fill-in.

plan is the load on the collision hall ceiling. Engineering studies are in progress. Until the full calculation is available, we argue that the load on the ceiling will be acceptable, because we would be trading the weight of main ring shield for a much shorter length of muon steel.

The steel shielding for the main ring currently runs the length of the hall and is suspended directly from the ceiling at a position slightly off of the detector centerline. (See Fig. 10.4). The load of a two foot thick slab of steel is approximately the same as the equivalent length of shielding. Thus we would be trading the load of the main ring shield for the load

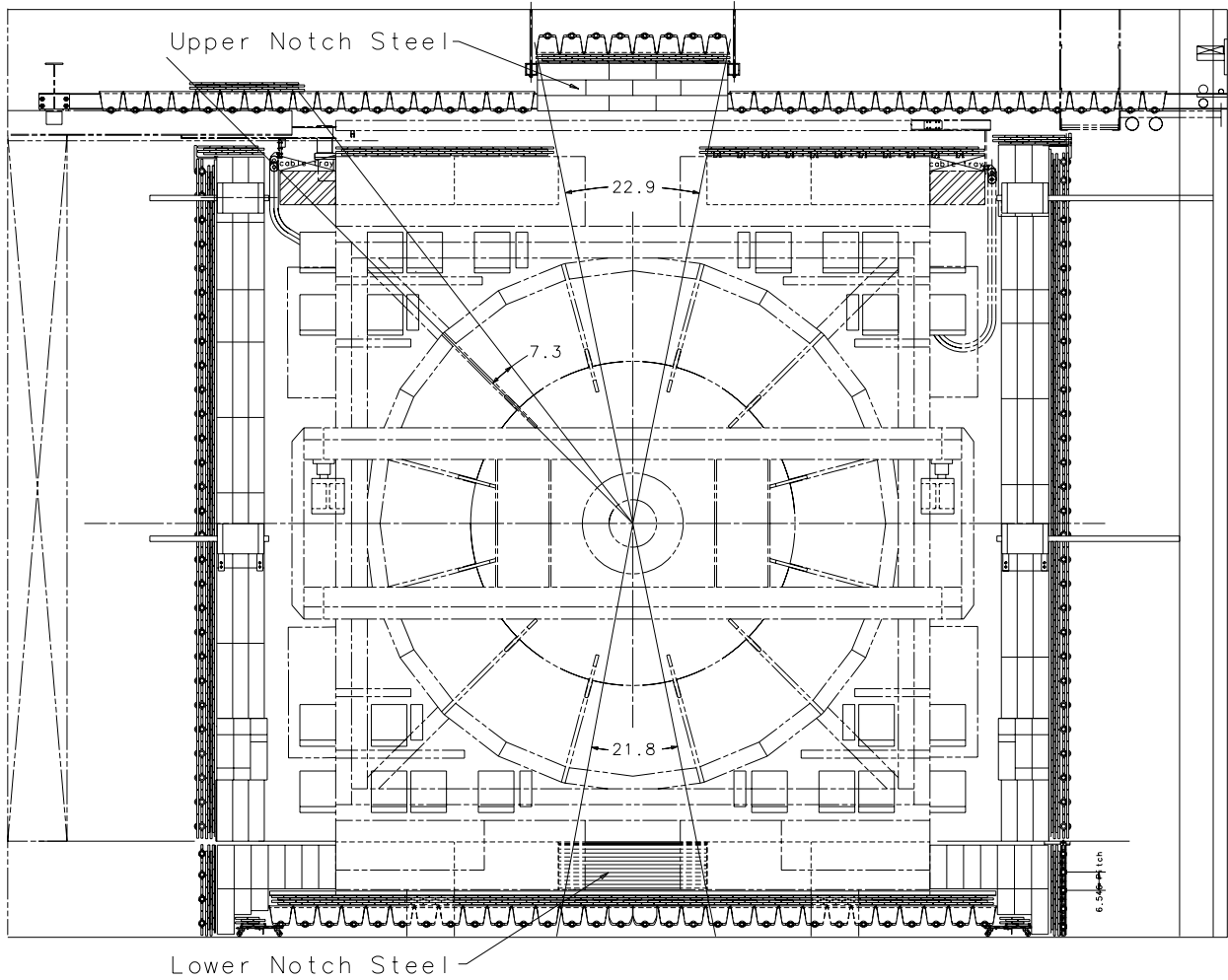


Figure 10.4: Configuration of the Central Muon Upgrade detector (CMP), Upgrade Scintillator (CSP) and steel absorber in Run II. On the walls the circles are the ends of PMTs. On the top and bottom the trapezoids are the lightguides viewed end-on.

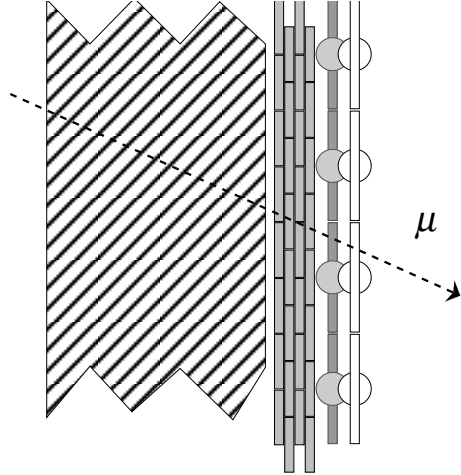


Figure 10.5: Detail showing the configuration of steel, chambers and counters for the Central Muon Upgrade walls. A muon track is drawn to establish the interaction point. Counter readout is located at $z=0$. Counters layers are offset from the chambers and from each other in x to allow overlapping light guides and PMTs, minimizing the space required.

of the steel absorber, but over a much shorter length, and moving the loading point slightly to the center of the detector, reducing the overall load on the ceiling.

Table 10.3 gives a summary of the relevant parameters for three CMP mounting alternatives at the top of the detector. For installation at ceiling height, we would increase the current load by a factor of 1.3 for a length of 21 feet over the central detector, but everywhere else, the load is gone. The impact on the detectors is shown in Table 10.4. The number of additional stacks is 4-5 and the decrease in acceptance due to the increased radius is very small.

As with the additions on the top, placing steel in the bottom yoke gap precludes access to the PMTs for the central calorimeter in bottom notch wedges. In addition, the procedure for closing the central arches uses an “observer” in this notch to guide the closing. We nevertheless propose to finish CMP in this region as proposed in the baseline plan. We will permanently install steel in the notch and chambers beneath. The chambers in the notch will be installed in the same manner as on the north and south return yokes. On the bottom, we solve the difficulties noted

above as follows:

- We will eliminate the need for an observer in the notch by upgrading the guide and control system for moving the arches.
- Access to the PMTs for the lower notch wedges will be provided from above rather than below. For access to the PMTs (a rare occasion) an arch will be pulled; personnel will go through the hole exposed at the center of the arch and drop down to the PMT from above.

Because adding carbon steel in either of the regions between yoke gaps has the potential to change the return flux, and because any change in the return flux will change the forces on the plug and could conceivably change the magnetic field in the central tracker, we choose to use stainless steel for these regions. We believe that the field changes with carbon steel would probably be small, but our knowledge of the magnetic field has been hard won and the cost of regenerating it with a different magnetic configuration would be much larger than the cost of using non-magnetic (stainless) steel in the bottom notch.

On the top, since the additions are above the return yoke, carbon steel is acceptable. We currently have the analog of the top yoke extensions at the bottom. This steel is magnetic and is separated from the central detector by a thin layer of G10 for electrical isolation. We propose to construct the top yoke extensions in the same way.

Completing the Upgrade scintillator is substantially less difficult. These counters are necessary to identify the beam crossing of the muon track. As shown in Figures 10.4 and 10.5, scintillator was installed on the two steel walls before Run Ib. The top and bottom regions must still be instrumented. The counters will be installed as close to the chambers as possible to minimize the difficulties in matching. Note that there are design problems with the counters that are not faced with the chambers. For full efficiency the counters must be as long as the chambers, but the counter light guide extends beyond the end of the counter.

10.4.2 Completion of the Central Muon Extension and Extension Scintillator

Completion of the Central Muon Extension (CMX) and Scintillator (CSX) requires:

	Increase in CMP coverage	Fraction of CMU with CMP coverage	number of stacks needed	Volume of steel (ft ³)
1	1.186	0.830	12	263
2	1.171	0.839	16	323
3	1.164	0.824	17	360

Table 10.4: Comparison of the 3 alternatives for filling the top yoke gap. The first column is the ratio of the Run II CMP coverage to the Ib coverage. The second column is the fraction of CMU covered by CMP. For Run Ib this is 0.703. The third and fourth column give the number of stacks (4-chamber unit) needed to instrument the gap and the volume of steel needed to provide 2 feet of absorber respectively.

- Chambers to instrument the top 30 degrees (2 wedges) in phi on the west side of the detector
- Chambers to instrument the bottom 90 degrees (6 wedges) of phi

These bottom detectors, commonly called the “mini-skirt”, are shown in Fig. 10.7. The chambers penetrate the nominal floor of the collision hall and require a different geometrical configuration than that of the upper 270 degrees. (See Fig. 10.6.) The conical geometry will not work.

The design of the mechanical support structure for the upper two wedges was completed before the beginning of Run Ia in 1992. The parts were also fabricated. The wedges were not installed due to mechanical interference between the upper surface of the mechanical support structure and the main ring shielding. Installation of the detectors in Run II requires the removal of one wedge on the north-west CMX stand and its subsequent reinstallation. The height of the stands requires that this take place in the collision hall.

The top wedges on the east side interfere with the cryogenics system for the CDF solenoid. Installation of additional detectors here would require a different configuration for the cryogenics or for the chambers. We do not plan to instrument this region for Run II.

The design, parts, and fabrication for the mini-skirt are complete at the time of this report. The chamber cross section is identical to that of the already installed chambers. The counters cover a smaller part of azimuth (6 per 15° wedge, as opposed to 4 in the rest of the detector). The geometrical arrangement of the detector is also slightly different. Instead of lying on a truncated cone, the chambers

form a flat pin-wheel structure with the wire lying along the spokes of the pin-wheel. There is only one layer of counters on the inner surface; the counters have a PMT on each end to allow the computation of a mean-time. The chamber wire and counter mid-planes are at a constant phi as in the rest of the detector.

The chambers and counters at the middle of the detector are shorter than the nominal length due to interferences with the detector sub-floor. This slightly reduces the coverage of the detector. The chambers and counters are glued into “wedgelets” consisting of 8 layers of chambers and 1 layer of counter. The wedgelets slide into place on a frame that rests partly on the nominal collision hall floor and partly on the sub-floor (Fig. 10.7 and 10.6).

10.5 Front-End Electronics

The front-end electronics for the Central Muon Detector will be upgraded for Run II. To survive the higher luminosity and event rates, the CMU gain will be reduced and the chambers will operate in proportional rather than limited-streamer mode. New pre-amplifiers and ASDs are being developed to match the dynamic range of the CMU chamber. Additionally, the wire ganging scheme will be changed to provide finer granularity in the position information at the trigger level, allowing tighter matching between muon “stubs”² and central tracks, which will improve purity. The ganging is performed on the CMU end electronics. When the front-end upgrades for

²We will call the short tracks reconstructed in the muon chambers “stubs” to distinguish them from tracks reconstructed in the central tracker.

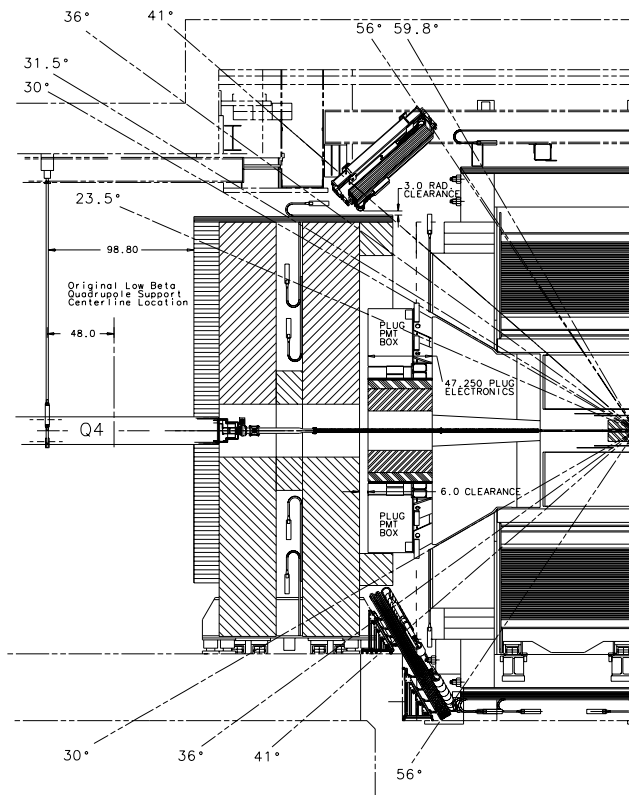


Figure 10.6: Side view showing the placement of chambers to complete the CMX coverage. Note the lower CMX detectors are supported on the floor and sub-floor. The IMU barrel chambers and scintillation counters, the toroid counters and the endwall counters are also shown.

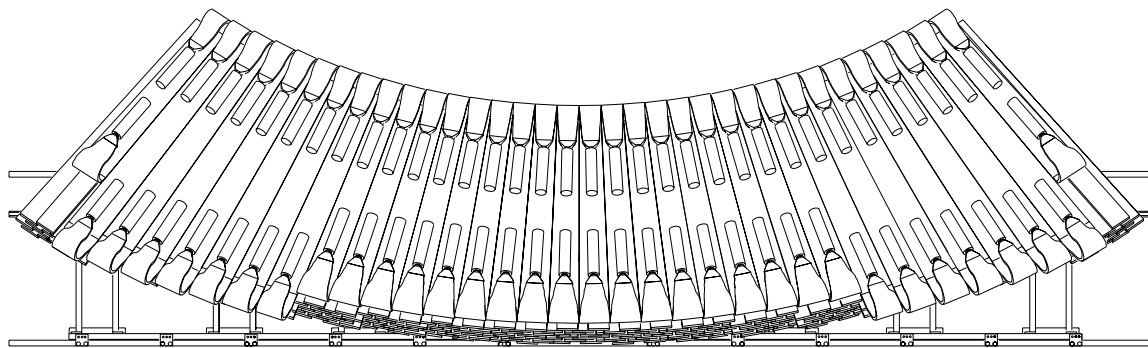


Figure 10.7: Lower chambers for the Central Muon Extension and Scintillators.

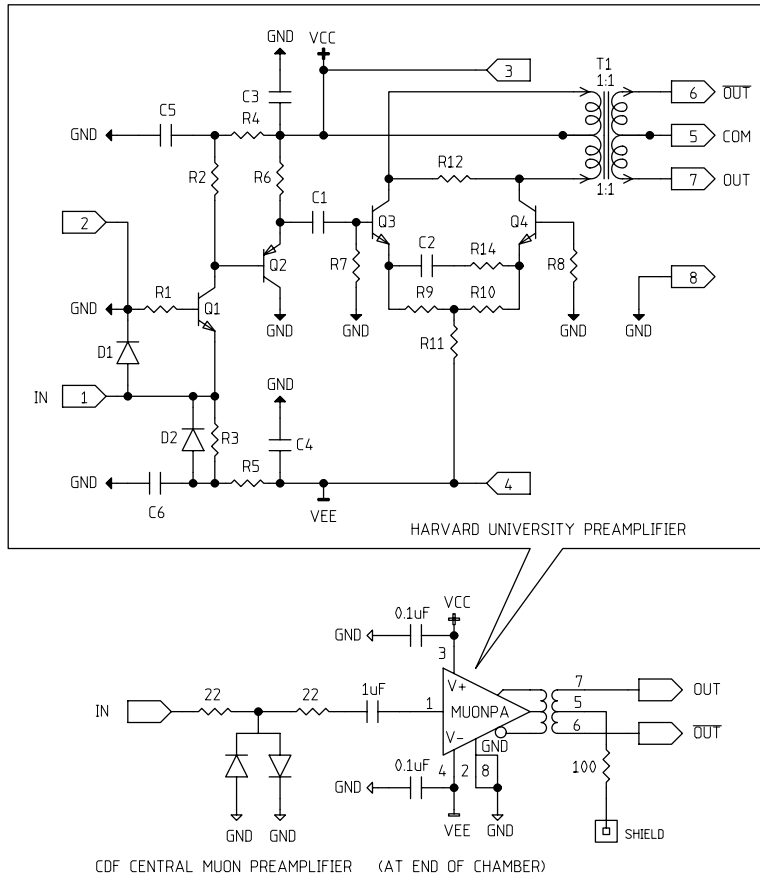


Figure 10.8: Hybrid pre-amp circuit for the Run II Central Muon detector readout

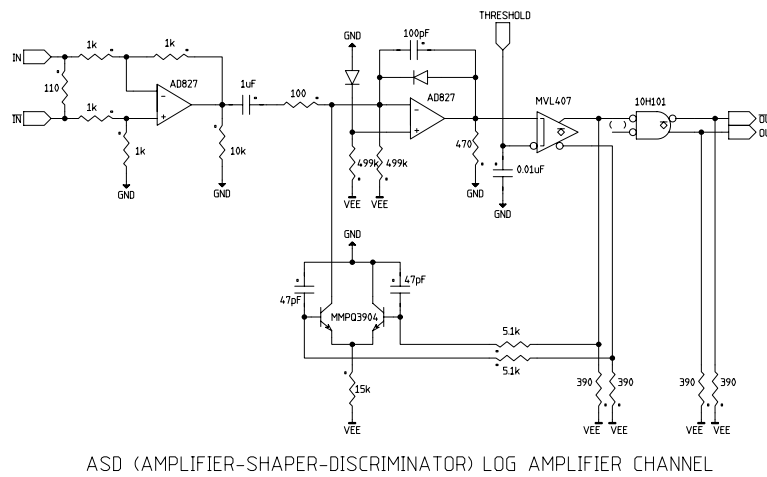


Figure 10.9: ASD/ToT circuit for the Run II Central Muon detector readout

Run II are complete, the readout for the three muon drift-tubes systems will be identical in concept and nearly the same in implementation. The two counter readout systems will similarly be identical conceptually and very similar in implementation.

The detector readout for CMP and CMX consists of a chamber-mounted pre-amplifier, an amplifier-shaper-discriminator card in the collision hall converting the analog signal to a logic-level signal. The signal is digitized by TDC cards in the counting room. The chamber, pre-amplifier, and ASD for the CMP and CMX are identical with the exception of chamber length. The only change planned in the read-out is to change the pre-amplifier mother-board system (not the pre-amplifier) for the Central Muon Upgrade detector.

The read-out of the counters consists of a photo-multiplier feeding a discriminator in the counting room. The discriminated hit signals for the CSP go directly to a TDC. The discriminated hit signals for the overlapping extension scintillator counters are input to a board for computing the mean time of the coincidence signal. This signal is then sent to a TDC.

Chambers and counters use the same TDC unit. In order to accommodate the pipelined DAQ structure and trigger buffering scheme, a new TDC is being developed to replace the current LeCroy 1879 module. The TDC is described in Secs. 11.3-11.4.

10.5.1 Changes in the Central Muon Upgrade Front-End Electronics

The Central Muon System (CMU) has proven to be a reliable and efficient detection device throughout Run I. In Run I the CMU drift chambers were operated in the limited streamer mode. In past runs we have experienced some minor difficulty in keeping the chambers running due to glow mode current runaway induced by high particle fluxes. Additionally, the chambers are aging. For these reasons we have decided to reduce the gain of the system and operate in the proportional regime, for the high luminosity running of Run II. In order to implement this we need to recoup the gain by installing pre-amplifiers on the chambers. The outputs of the pre-amps will drive amplifier-shaper-discriminator(ASD) cards, followed by TDC's.

The transverse coordinate is measured using the usual distance-to-drift-time relation; there is no change from the Run I scheme, and the resolution

is unchanged. The z -coordinate is measured using charge division as before, but in the new scheme the charge is determined by time-over-threshold (TOT) instead of charge-to-voltage conversion. The z -resolution is degraded with respect to Run I due to the significantly lower chamber gain. Cosmic ray test stand measurements show a resolution of 10 cm, which is adequate to pin down the muon to one trigger tower, and is comparable to our most stringent physics analysis cuts applied to high p_T muons. For $J/\psi \rightarrow \mu^+\mu^-$ decays, the multiple scattering for the muon is typically around 8 cm, so the worsened z resolution will have a slight impact: the background level may rise by a few percent.

10.5.1.1 Pre-amplifier

The pre-amplifiers reside on mother boards attached to the end of the CMU chambers. The mother board is a redesign of the original CMU end board with provisions for pre-amp power and additional calibration pulse inputs. The pre-amp has a low-impedance grounded-base input followed by amplification and an output stage providing differential signals to a 100 Ω impedance transmission line. The differential output reduces common mode noise, an advantage in the relatively noisy CDF environment. A schematic diagram of the pre-amplifier is shown in Fig. 10.8.

10.5.1.2 ASD/TOT

The amplifier-shaper-discriminator and time-over-threshold circuit (ASD/TOT) accepts signals from the CMU pre-amplifiers via a 5 meter 100 Ω flat ribbon cable. The ASD cards reside in a VME crate at the back of each 15 degree wedge. The signals are differentially received and amplified. The current is integrated on a capacitor and then discharged with a constant current source. The output of the following discriminator is then linearly related to the total charge. The transverse coordinate of the muon track is given by the leading edge of the discriminator whereas the z -coordinate is related to the ratio of the TOT's of adjacent channels. The outputs of the discriminators are sent via differential ECL signals to TDCs residing in the first floor counting room. A schematic diagram of the ASD/TOT circuit is shown in Fig. 10.9.

10.5.1.3 Bunch Crossing Ambiguity

Since the maximum drift time of the CMU chambers is on the order of 700 ns and the bunch crossing separation is 132 ns, one does not know which of six bunches the muon belongs to. In order to resolve this ambiguity a muon track will be associated with six bunches and, as such, can contribute to a Level 1 trigger with any of these. The correct bunch within the six must be determined by associating the muon stub with an XFT track and appropriate calorimeter hit: TDC's on the Central Hadron Calorimeter are capable of resolving a single bunch crossing. Additionally, triggers requiring CMP confirmation (e.g. high p_T muons from W decay) will have their crossing identified by the CSP scintillators.

10.5.2 Changes in the Central Muon Upgrade Front-End Electronics

We have had intermittent problems with oscillations since the chambers were installed. It is now clear that these problems were due to design flaws in the preamplifier circuit boards. We reduced the severity of the problem in Run Ib by installing relays in the pre-amplifier power distribution so that we can shut off individual channels from the counting room. This allows us to stop the oscillations without making an access, and has reduced the amount of bad data due to CMP oscillations from about 4% in Run Ia to well under 1% in Run Ib. Nevertheless, lost data is lost data: 1% of the Run II goal of 2fb^{-1} is equivalent to the entire Run Ia dataset.

For Run II, we wish to solve this problem at its root. We have completed a new design for these pre-amplifier boards. Ten prototype boards were installed and tested at the end of Run Ib. They performed well during the limited data-taking. No oscillations were found during the 4 month running period. We plan to replace all the pre-amplifier boards with ones using the improved design for Run II.

10.6 Intermediate Muon Detection

10.6.1 Overview

The importance of lepton identification does not stop at $\eta = 1$, and to that end CDF has designed a system that builds on the successes of CDF's central muon identification and on a major strength of CDF II,

charged particle tracking at mid-rapidity. The IMU is designed to trigger on muons with $|\eta| \leq 1.5$ and to identify off-line muons with $|\eta| \leq 2.0$. The heart of the detector is a barrel of CMP-like chambers and CSP-like scintillation counters mounted on the outer radius of the FMU toroids. Additionally, there are pinwheels of counters on the endwall and between the toroids for triggering. A muon is identified by a stub in the chambers, with a time-stamp provided by the barrel counters in coincidence with the pinwheel counter projective with the vertex. Note that in all cases, there is a substantial volume of steel between the barrel and pinwheel counters.

Unfortunately, we cannot extrapolate Run II IMU performance from Run I IMU performance, but we can compare the IMU to the existing detectors. The IMU is behind 6.2-20 interaction lengths of steel, on average more shielding than CMP. Figure 10.10 shows the amount of absorber between the detector and interaction vertex as a function of η . The IMU has smaller chambers, which reduces the mean occupancy for two reasons. First is the geometric factor - each counter covers less solid angle. Second is that the maximum drift time is shorter, so the number of effective interactions the IMU sees is smaller than the number the CMU sees. Additionally, having a set of scintillation counters projective with the IMU barrel provide additional redundancy. Monte Carlo studies are underway. Preliminary results indicate that occupancies even at 2×10^{32} are well below acceptable limits.

10.6.2 Toroid Modifications

Three modifications to the existing toroidal magnets will be made. First, the toroids will be pushed from their present position 5.5 m closer to the interaction. This will involve construction of a toroid movement system similar to that for the present CMP. This increases the solid angle subtended by the IMU. Next, a ring of steel ~ 60 cm square in cross-section will be welded onto the inner face of the toroids. This ring will provide shielding for the IMU barrel chambers, and will additionally shield the CMX from tertiary particles. Monte Carlo studies indicate that this modification reduces the trigger rate by a factor of 6. Finally, the toroids will not be energized. Momentum will be measured using the solenoidal magnetic field. The silicon (SVX and ISL) gives superior momentum resolution if either of the following conditions is true:

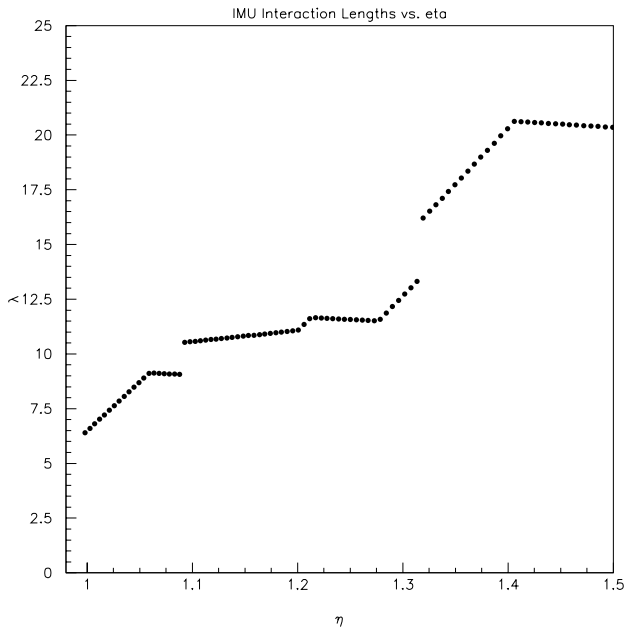


Figure 10.10: The amount of steel absorber (measured in interaction lengths) between the IMU Barrel and the interaction point, as a function of pseudo-rapidity.

$$p_T(\mu) \leq 50 \text{ GeV or } |\eta(\mu)| \leq 1.5.$$

10.6.3 IMU Barrel Chambers and Counters

Surrounding the toroids in a barrel geometry will be 1728 chambers, 864 on the east side of the detector, and 864 on the west. The chambers are 11.9' long, 1" deep, and 3.3" wide, with each chamber covering 1.25° of azimuth. The chambers are assembled in stacks 4 deep (in radius), with the second and fourth layers staggered relative to the first and third to resolve hit assignment ambiguities. Apart from size, these chambers are identical to the CMP chambers described above, single wires through aluminum extrusions, with cathode strips for field shaping. The preamplifier will be similar to the that used in the CMP, and the system will use the same ASD's and TDC's as the CMP and CMX. The intent is to minimize the development and engineering necessary for this system and to take advantage of the excellent

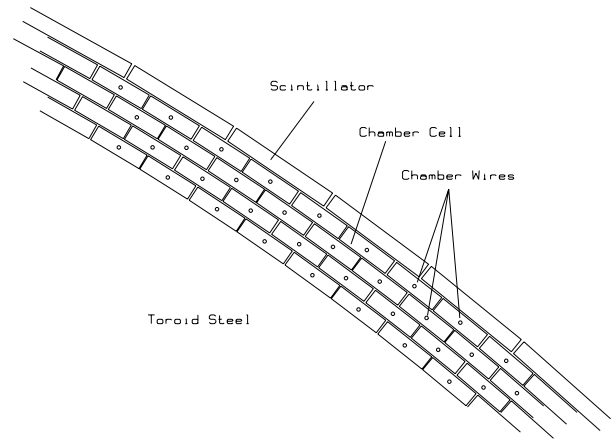


Figure 10.11: A detailed section of the IMU Barrel, showing several chamber cells and corresponding scintillator.

performance of the existing CMP detector and read-out chain.

These chambers cover the top 270 degrees of the toroids; the floor interferes with installation of the bottom quarter. The 3.8 m of steel in the toroids provides substantial shielding from spray off the beam-line.

The 3.3" width of these chambers implies a maximum drift time of about 1 microsecond, longer than the beam crossing times of 396 ns or 132 ns. To identify which beam crossing produced the muon, an array of rectangular scintillator counters is installed just outside of the barrel IMU detector. As with the CSP, each counter covers two chambers in ϕ and half a chamber in η : one set of counters covers between $\eta=1.0$ and 1.25 and the other set of counters covers between $\eta=1.25$ and 1.5. Note that this design provides some η information at the trigger level. There are 432 counters on the barrel (216 on each side), read out by phototubes mounted at the outside ends. Readout will be identical to the CSP.

Figures 10.11, 10.6 and 10.12 show the IMU Barrel in various views.

10.6.4 IMU Toroid Counters

In the CMX/CSX, there are two scintillation counters per chamber stack, one on the inner and one on the outer radius of the stack. The IMU also has two layers of scintillator everywhere, but rather than mounting the second set within inches of the first, the second set in the IMU is separated by substantial

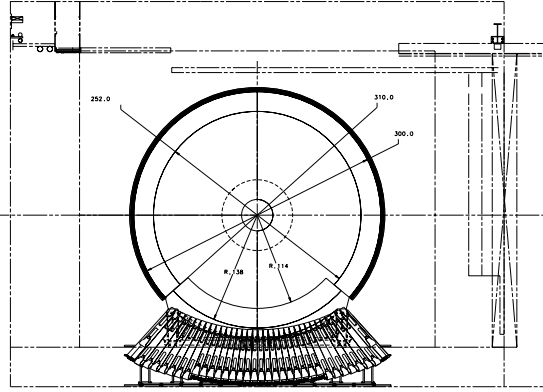


Figure 10.12: Elevation view of the IMU Barrel, viewed along the beam axis. The IMU chambers and scintillators are represented by the outer circle around the toroids. Toroid coils (not shown) may interfere with IMU installation at $\pm 45^\circ$ and $\pm 135^\circ$. The CMX lower 90° section is also shown.

distance and steel from the first set. This adds the requirement that the coincidence between two counters have a projective geometry, and that any single particle that causes the coincidence be able to penetrate a large volume of steel; background triggers caused by soft tertiary hadrons, a problem early on in the CMX, are strongly suppressed in this design.

One pinwheel of 144 counters is mounted between the inner and outer toroids, with a granularity of 5° in ϕ and covering $\eta = 1.3 - 1.5$. A second set is mounted at lower radius, covering $\eta = 1.5 - 2.0$, also with 5° ϕ segmentation. The inner set is used for identifying high p_T isolated tracks as muons. Presently, CDF considers isolated high p_T tracks with minimum ionizing energy deposition in the calorimeter as possible muon candidates. The purity of this sample can be substantially improved by requiring that the candidate penetrate an additional meter of steel and be detected by the $\eta = 1.5 - 2.0$ counters. The 288 toroid counters use the phototubes and bases of the existing FMU scintillator counters, although the aging original scintillator (now over a decade old) will be replaced with new plastic.

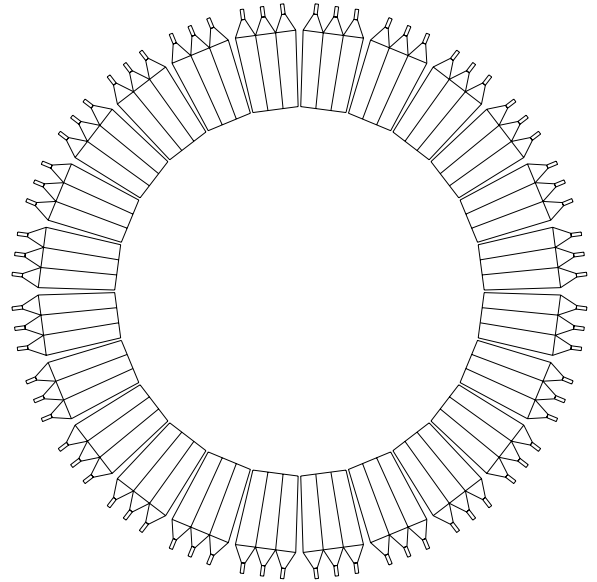


Figure 10.13: The geometry of the endwall muon counters. The small gaps every 15° correspond to the wedge boundaries on the endwall. The toroid counters are similar, except that the gaps are absent.

10.6.5 IMU Endwall Counters

The toroid counters cannot cover $\eta \leq 1.3$, so we will install another pinwheel of 144 counters on the endwall calorimeter. These counters are 5° wide and cover $\eta = 1.0 - 1.3$. Space on the endwall is tight, but there is room for 1" thick scintillator. Additional space for the photomultiplier tubes is available just outside the endwall calorimeter (in radius). Test counters were installed on the endwall and operated during the last four months of Run I. Data from these counters indicates that the singles rates are not too high in this region of the detector, even for counters in close proximity to the endwall ^{137}Cs source.

10.6.6 Triggering on $\eta \geq 1$ Muons

The ϕ granularity of the IMU is designed to match the granularity of the trigger. The XFT reports tracks in 1.25° bins, so the chambers cover 1.25° in phi. The barrel scintillation counters each cover two XFT ϕ bins, (2.5°) and the endwall and toroid planar counters each cover 4. (5°) There are four elements in coincidence that are necessary to form a trigger:

- A "stub" of at least 3 hits in the IMU chambers. The slope $d\phi/dr$ can be measured by the drift time differences between the hits in a manner sim-

ilar to the present CMU. While in the CMU, the slope is a function of the p_T of the muons, in the IMU, muons have traversed a significant fraction of the magnet’s return field so all muons from the interaction point are close to radial. Background stubs from the typical sources (spray from the beampipe, albedo, etc.) are not necessarily radial, so the stub slope extracted from timing information allows us to reject background.

- A scintillator hit in the barrel scintillator. This identifies which interaction produced the muons.

- A scintillator hit in the appropriate pinwheel counter. This rejects against accidental coincidences between real particles at the IMU barrel, and real high p_T tracks that were unassociated with the particles detected in the IMU.

- A track found in the appropriate ϕ bin in the XFT. At the present time, the XFT reports tracks with $|\eta| \leq 1.2$, so the trigger is limited to this region. (As more forward tracks become available at the trigger level, however, the IMU’s triggering capability will be likewise extended.) Unlike the other muon systems, a crude z matching requirement can be imposed between the track and the muon stub at the trigger level. Since the XFT only finds tracks with $|\eta| < 1.2$, we can require that the $\eta = 1.0 - 1.25$ barrel scintillator (as opposed to the scintillator covering $\eta = 1.25 - 1.5$) be hit. Because tracks with $\eta = 1.0 - 1.2$ will traverse only the innermost three axial superlayers in the COT, we can require that the outermost COT superlayer be *missed*.

10.6.7 Summary

To summarize, the IMU is a system designed for excellent identification of muons in the range $\eta = 1.0 - 2.0$, with emphasis on the low rapidity region. It has several features designed to reject background both offline and at the trigger level: a large volume of steel shielding, the ability to require a coincidence between counters separated by shielding and distance, and the ability to measure stub angles and thus to reject stubs that were not produced by muons from the interaction point. The system is extremely similar to the existing muon systems, both in mechanical and electrical design, using the best features of each of the central muon systems, and saving both cost and effort in detector development. Initially, the IMU can be used to trigger on muons with $|\eta| \leq 1.2$, with the ability to expand to 1.5 as soon as tracks

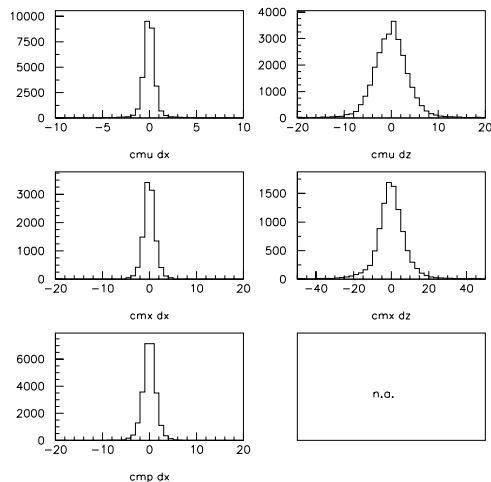


Figure 10.14: Resolution for matching between muon stubs and extrapolated tracks measured with high p_T muons from W and Z decays.

at these rapidities become available at the trigger level. Although we do not propose this as part of this Report, the possibility of an upgrade involving energized toroids and additional detector elements to track muons through the toroids is not precluded by this design. Such a system could tag muons beyond $\eta = 2.0$ and trigger beyond $\eta = 1.5$.

10.7 Performance: Extrapolation From Run I

The existing muon detectors have performed admirably during Run I. Figure 10.14 shows the x and z residuals for muons from W and Z decay in the CMU, CMX and CMP. Figure 10.15 shows the J/ψ mass from muons with both legs in the CMU, at least one with CMP confirmation and at least one in the CMX. In all three of these examples, the background to the J/ψ peak is quite low, and although the background is lowest when upgrade confirmation is required, it is quite possible to do excellent physics with the signal-to-noise ratio in any of these cases.

We would obviously like to maintain this performance in the Run II era, and we believe that the proposed system will do this. We briefly review here the expected effects of Run II luminosities and beam conditions on detector aging, occupancy, and offline reconstruction. We do not discuss the performance

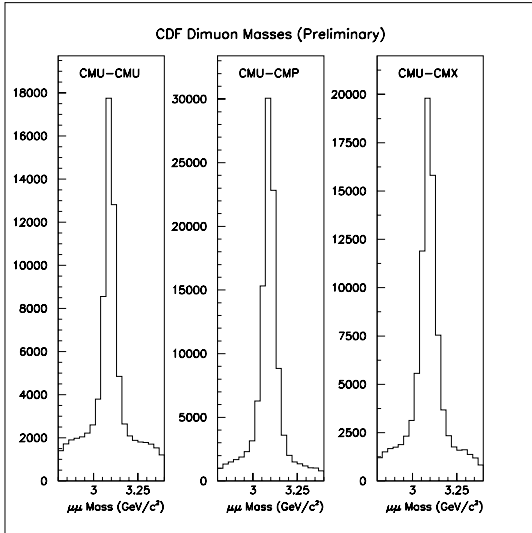


Figure 10.15: Reconstructed J/ψ mass for various detector decay topologies.

of the trigger, other than to comment that 2/3 of the CMU trigger rate comes from the 1/3 of the detector without CMP confirmation. Completing the CMP coverage will therefore provide substantial purity improvement at the trigger level. The trigger is discussed in Sec. 12.

Most ($\geq 95\%$) of the ionization detected in the CDF muon system is not from Tevatron produced particles, either from $p\bar{p}$ collisions or beam halo, but rather comes from the Main Ring. We have monitored the total ionization in the chambers, and the dominant time structure is the Main Ring cycle, with the currents highest at injection, transition, and extraction. We have compared single hit chamber occupancies from (otherwise identical) runs with the main ring on and off, and they differ by between one and two orders of magnitude.³ Clearly the Main Ring is what these detectors see, and the Tevatron is a perturbation on top of that.

We have examined the CMP and CMX for signs of main ring induced aging by comparing chambers near the main ring (highest integrated flux) to chambers near or under the floor, (lowest integrated flux) and to chambers never exposed to the beam. We see no difference in pulse characteristics and conclude that there is no significant radiation induced aging in these

³The largest variation is between in-time occupancies and between total currents. This is not unexpected; one requires coincidence with the beam crossing, and the other does not.

occupancy	CMU	CMP	CSP	CMX	CSX
Run I	0.01	0.9	0.2	0.5	0.02
Run II	0.007	0.04	0.01	0.2	0.01

Table 10.5: Channel occupancy (%/channel/event) in minimum bias events. These are computed from Ib data, corrected to 1 minimum bias event per crossing. The reduction in rate expected when the main ring is removed is also included. This is computed from the top-bottom asymmetry in the azimuthal hit occupancy distribution.

systems.

A similar comparison for the CMU shows a decrease in the single hit efficiency of a few percent. This is not large enough to be visible in the muon finding efficiency (where we require 3 of 4 hits) with the Run I data. Reducing the CMU gain by a factor of 30 or so will slow this aging by the same factor, and removing the main ring will slow it an additional factor of 100 or more. Even going to very high luminosities is quite safe. More than 90% of the charge that will ever be collected from the CMU has already been deposited.

In Run II, with the Main Ring gone and the beam pipe shielded (see Sec. 14.4), the environment of the central muon detectors will be much less harsh. The raw detector occupancy measured online in Run Ib minimum-bias events [6] is given in the first row of Table 10.7, and the occupancy of stubs in minimum-bias events is given in Table 10.7. We expect substantially reduced occupancy (Tables 10.7 and 10.7) in Run II. In CMU and CMP the expected reduction is estimated from measurements of the top-bottom asymmetry in the azimuthal occupancy distribution. In CMX the expected reduction factor is estimated from the ratio of in-time to out-of-time stubs. This removes both the main ring component and some fraction of the particles from interactions in the beam pipe.⁴ The expected Run II occupancies are shown in the bottom lines of Tables 10.7 and 10.7, and represent significant improvements over the Run I situation.

Shielding will have an even larger effect since the timing cut does not perfectly separate signal and noise. A preliminary shielding plan for CDF II is

⁴The timing cut implemented corresponds to that used in the trigger and is corrected for the corresponding loss in efficiency (15%).

occupancy	CMU	CMP	CMX
Run I	0.034	0.14	0.35
Run II	0.023	0.0084	0.026

Table 10.6: Mean stub occupancy (stubs/event) in minimum bias events. These are computed from Ib data, corrected to 1 minimum bias event per crossing. The potential improvement when the main ring is removed and shielding can be installed around the beam pipe is also given. The occupancy is not Poisson distributed: the fraction of events with no stubs is much larger than $e^{-\langle n \rangle}$.

bunch	\bar{N}	CMU	CMP	CMX
132 ns	2	2.2%	0.39%	0.71%
396 ns	5	1.8%	0.33%	0.59%

Table 10.7: Probability of a stub from an underlying minimum bias event overlapping with a stub of interest in a physics event at a luminosity of $2 \times 10^{32} \text{ cm}^{-2} \text{ s}^{-1}$.

discussed in Sec. 14.4. We estimate that the installation of shielding around the beam pipe will reduce rates by a factor between 50 and 100. Additionally, the additional steel welded onto the toroids for the IMU will substantially reduce the background stubs in the CMX.

There is also a concern that offline reconstruction will be difficult because the muon chambers integrate over several crossings. However, the CMX and the CMP have scintillators that will time stamp the crossing with the muons (i.e. will identify which beam crossing is associated with the muon of interest). The CMU can be correlated with times from TDC's attached to the central hadron calorimeter readout, and the fast drift times in the tracking chambers will allow unambiguous association of a matching track with a given beam crossing. As a figure of merit we calculate the probability that a muon track of interest is obscured by another in an underlying event. We consider the muon track to be "obscured" when two particles overlap within the maximum drift time of the chamber in a unit of azimuth defined by the scintillator used to identify the beam crossing.⁵ This probability is plotted as a function of the number of underlying minimum bias events in

⁵This figure of merit arises naturally from the simplest extension of the current stub finding algorithms to Run II conditions.

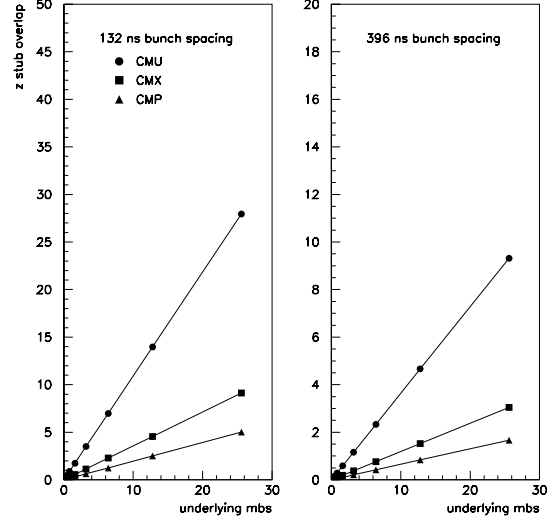


Figure 10.16: Probability of a stub from an underlying minimum bias event overlapping with a stub of interest in a physics event.

Figure 10.16 and listed for the Run II crossing rates at $2 \times 10^{32} \text{ cm}^{-2} \text{ s}^{-1}$ in Table 10.7. The probability of a pure stub overlap is a few %. In these situations with overlap we will be able to resolve the two tracks with a slightly more complicated reconstruction algorithm which will be slower for this rare category of events. We conclude that this kind of overlap is not a problem.

To summarize, we expect that the improvements to the CDF II muon systems outlined here will substantially enhance Run II performance over Run I:

- The Main Ring will be removed, decreasing occupancy.
- The CMX will be shielded by the IMU, further decreasing occupancy.
- The ϕ coverage of the CMP will be increased. Scintillator will identify each muon's bunch crossing.
- The ϕ coverage of the CMX will be increased.
- The new IMU will allow muons to be identified out to $\eta = 2.0$, and triggered on out to $\eta = 1.5$. ($\eta = 1.2$ at the beginning of Run II)

Bibliography

- [1] K. Byrum, et. al., “The CDF Forward Muon System”, NIM A268 (1988) pp. 46-49.
- [2] G. Ascoli, et. al., “The CDF Central Muon Detector”, NIM A268 (1988) pp. 33-40.
- [3] The CDF Collaboration, “Proposal for an Upgraded CDF Detector”, CDF Internal Note 1332 (PinkBook), December, 1990.
- [4] Brandenburg, et. al., “A Proposal to Upgrade the CDF Muon System”, CDF Internal Note 773, October, 1988.
- [5] Fermilab, Harvard, Illinois, Pisa, Osaka, Tsukuba, Pisa, Frascati, etc., “The 1992 CDF Muon System Upgrade”, CDF Internal Note 2858, October, 1994
- [6] L. Nodulman, “Detector Counting Rates in the 94-96 Run”, CDF Internal Note 3643, April, 1996.
- [7] S. Abachi, et. al., “The D0 Upgrade: Forward Preshower, Muon System and Level 2 Trigger”, Fermilab Technical Note FERMILAB-FN641, April, 1996.